Real-Time Kinetic Studies on the Interaction of Transforming Growth Factor α with the Epidermal Growth Factor Receptor Extracellular Domain Reveal a Conformational Change Model†

Gregory De Crescenzo,‡ Suzanne Grothe,‡ Robert Lortie, Maria T. Debanne, and Maureen O'Connor-McCourt*

Biotechnology Research Institute, National Research Council (Canada), 6100, Royalmount Avenue, Montreal, Quebec, Canada H4P 2R2

Received December 30, 1999; Revised Manuscript Received April 3, 2000

ABSTRACT: Transforming growth factor α (TGF-α), epidermal growth factor (EGF), and related factors mediate their biological effects by binding to the extracellular domain of the EGF receptor, which leads to activation of the receptor's cytoplasmic tyrosine kinase activity. Much remains to be determined, however, about the detailed molecular mechanism involved in this ligand-induced receptor activation. The determination of the binding mechanism and the related thermodynamic and kinetic parameters are of prime importance. To do so, we have used a surface plasmon resonance-based biosensor (the BIAcore) that allows the real-time recording of the interaction between TGF-α and the extracellular domain of the EGF receptor. By immobilizing different biotinylated derivatives of TGF-α on the sensor chip surface, we demonstrated that the N-terminus of TGF-α is not directly involved in receptor binding. By optimizing experimental conditions and interpreting the biosensor results by several data analysis methods, we were able to show that the data do not fit a simple binding model. Through global analysis of the data using a numerical integration method, we tested several binding mechanisms for the TGF-α/EGF receptor interaction and found that a conformational change model best fits the biosensor data. Our results, combined with other analyses, strongly support a receptor activation mechanism in which ligand binding results in a conformation-driven exposure of a dimerization site on the receptor.

Transforming growth factor α (TGF-α),[1] epidermal growth factor (EGF), and related factors are mitogens that mediate their biological effects by binding to and activating the EGF receptor. Once activated, the receptor transmits signals across the plasma membrane, which ultimately lead to cell growth and division (*1*, *2*). The EGF receptor is composed of three domains: the ligand-binding extracellular domain, a single transmembrane helix, and a tyrosine kinase cytoplasmic domain (*3*). Ligand binding induces receptor dimerization and simultaneous activation of its intrinsic tyrosine kinase activity. This activation results in the phosphorylation of tyrosine residues on a set of target proteins that include the EGF receptor cytoplasmic domain itself. This increase in tyrosine phosphorylation initiates a cascade of events that moves through the cytoplasm to the nucleus and results in effects on cell division and differentiation. Since the binding of ligand to the EGF receptor extracellular domain is the initial interaction in the EGF receptor response pathway, an elucidation of the molecular mechanism of this interaction is required for the rational design of agonists and/or antagonists to the EGF receptor.

Essential to our understanding of the molecular basis of ligand−receptor interactions is the determination of the thermodynamic and kinetic parameters associated with these binding events. The recent availability of optical biosensors, such as the surface plasmon resonance (SPR) detector (the BIAcore), allows for the detection of macromolecular interactions in real time. Rate constants that otherwise would have been difficult to obtain can now be measured. In a typical BIAcore experiment, one component (termed the ligand) is immobilized onto the dextran layer of the sensor chip in the system microflow cell. A solution containing the second interacting component (termed the analyte) is then flowed over the immobilized ligand. As the analyte and ligand interact, the mass at the sensor chip surface increases and this causes a refractive index change that is measured as a change in the SPR angle. The results are plotted in the form of a sensorgram (resonance units versus time), which consists of a wash-on phase that begins as soon as the analyte is injected over the surface and a wash-off phase that corresponds to the time point when the analyte solution is

† Supported by the Protein Engineering Network of Centres of Excellence (PENCE). This article bears the NRCC publication number 42952.

* To whom correspondence should be addressed. Tel: 514-496-6382. Fax: 514-496-5143. e-mail address: maureen.o'connor@nrc.ca.

‡ These authors contributed equally to this work.

[1] Abbreviations: TGF-α, transforming growth factor α; EGF, epidermal growth factor; SPR, surface plasmon resonance; NHS, *N*-hydroxysuccinimide; EDC, *N*-ethyl-*N*′-(3-dimethylaminopropyl)-carbodiimide hydrochloride; NHS-SS-biotin, sulfosuccinimido, 2-(biotinamido)ethyl-1,3-dithiopropionate; EGFR-ED, epidermal growth factor receptor extracellular domain; PMSF, phenylmethanesulfonyl fluoride; DMSO, dimethyl sulfoxide; TFA, trifluoroacetic acid; HPLC, high-performance liquid chromatography; EDTA, disodium ethylenediaminetetraacetate; HBS, *N*-(2-hydroxyethyl)piperazine-*N*′-2-ethanesulfonic acid (Hepes) buffered saline; IL-2, interleukin 2; PBS, phosphate-buffered saline; SAXS, small-angle X-ray scattering; BSA, bovine serum albumin; RU, resonance unit; MOI, multiplicity of infection; NMR, nuclear magnetic resonance; NOE, nuclear overhauser enhancement; HSQC, heteronuclear single quantum correlation.

10.1021/bi992987r CCC: $19.00 Published 2000 by the American Chemical Society
Published on Web 07/14/2000

replaced by buffer. We have adapted the BIAcore system for analyzing the interaction between TGF-α and the EGF receptor extracellular domain (EGFR-ED) by immobilizing TGF-α and flowing a solution of purified EGFR-ED.

At present, there are three methods available to calculate kinetic rate constants from biosensor data (*4*). These are (i) linearization (*5*), (ii) curve fitting with analytical integration (*6*), and (iii) curve fitting with numerical integration (*7*). Analysis by the linearization or integrated rate equation methods is sufficient for interpreting a simple bimolecular or Langmuir interaction. However, it has become apparent that most of the interactions that have been studied with biosensors yield data that do not fit this simple binding model, as evidenced by curved plots following linearization or by the inability to be fit by a single integrated equation. This behavior may be the result of physical effects that occur in the biosensor or alternatively may be indicative of the need for a more complex reaction mechanism to describe the interaction. By analyzing the biosensor data from the TGF-α/EGF receptor extracellular domain interaction by all three data analysis methods, we have been able to show that the data do not fit a simple binding model. It has recently been proposed that physical effects in the biosensor such as heterogeneity of the immobilized ligand may provide an explanation for the deviation of BIAcore data away from fitting a simple model more often than explanations requiring more complicated binding models (*8*). By varying experimental conditions and minimizing heterogeneity on the surface by immobilizing the ligand through a single site, we eliminate these proposed physical effects as an explanation for the nonconformity of the TGF-α/EGF receptor extracellular domain biosensor data.

On the basis of information derived from solution studies, we have proposed several binding mechanisms for the TGF-α/EGF receptor interaction that are more complicated than the simple bimolecular interaction model. These include (1) a model involving a conformational change or transformation of the complex following ligand binding [this model is based on solution data indicating that the ligand induces a conformational change in the receptor (*9*)]; (2) a model proposing the formation of a receptor dimer [this model was formulated on the basis of studies done by Brown et al. (*10*) and Lemmon et al. (*11*) indicating that receptor dimerization follows ligand binding]; and (3) a model involving the formation of a complex composed of one ligand and two monomers of receptor [this model is based on the behavior of the growth hormone receptor (*12*)]. Using the numerical integration method, we demonstrate that the conformational change model best fits the biosensor data.

EXPERIMENTAL PROCEDURES

Equipment and Reagents. Human TGF-α was purchased from Bachem Bioscience Inc.. Human EGF was purchased from Austral. Streptavidin and NHS-SS-biotin were purchased from Pierce. The amine coupling kit containing NHS, EDC, and 1 M ethanolamine, pH 8.5, and CM5 sensor chips were purchased from BIAcore Inc.

Production and Purification of the EGF Receptor Extracellular Domain. Recombinant baculovirus carrying the EGFR-ED cDNA was generated as previously described (*10*). Twenty liters of SF9 cells [$(5-10) \times 10^6$ cells/mL] grown in suspension (SF-900 medium) were infected with recombinant baculovirus at a MOI between 0.5 and 3. The culture supernatant containing the EGFR-ED was harvested at 72 h postinfection. The supernatant was either frozen after addition of PMSF (0.1 mM) and glycerol (10% v/v), or the EGFR-ED was immediately purified as previously described (*13*). The purity of EGFR-ED (more than 85%) was determined by densitometric scanning of Coomassie Blue stained gels and the concentration by the Lowry method after dialysis against PBS.

Biotinylation of TGF-α. Lyophilized TGF-α (50 μg) was dissolved at a concentration of 1 mg/mL in 0.1 M sodium bicarbonate, pH 8.5. NHS−SS-biotin (56 μg) was dissolved in DMSO and was added to the TGF-α solution. This represents a 10-fold molar excess of biotin over TGF-α. The mixture was incubated for 4 h at 25 °C after which 200 μL of 0.1% TFA was added. Free biotin, unbiotinylated TGF-α, and the different biotinylated derivatives of TGF-α were separated by reverse-phase HPLC on a C-18 column (Vydac) with a 18−40% acetonitrile gradient in 0.1% TFA over a 120 min period.

^{125}I Competition Binding Assay. Human EGF was iodinated by the chloramine T method as described (*14*). Competition of ^{125}I-EGF binding to the EGFR-ED was done by microtiter plate assay essentially as described previously (*10*). Briefly, the EGFR-ED was incubated with ^{125}I-EGF in assay buffer [150 mM NaCl, 10 mM Hepes, 0.1% (w/v) NaN_3, 0.1% (w/v) BSA, and 0.02% (v/v) Tween 20, pH 8.0] in the presence of increasing amounts of TGF-α or the biotinylated derivatives of TGF-α on removable microtiter wells precoated with a monoclonal antibody specific for the EGFR-ED. After a 3 h incubation at 37 °C, the unbound ^{125}I-EGF was removed by a single wash with assay buffer at room temperature. The amount of bound ^{125}I-EGF was determined with an LKB γ counter and, for each concentration of the competing molecule, is expressed as the percentage of binding obtained in the absence of competing molecule. When experiments were done in the presence of streptavidin, the biotinylated derivatives of TGF-α were preincubated with different concentrations of streptavidin for 1 h at room temperature in assay buffer prior to the incubation with ^{125}I-EGF.

Immobilization of TGF-α on the Sensor Chip Surface. Streptavidin was immobilized on the surface of a CM5 sensor chip by the standard amine coupling procedure. All BIAcore experiments were done at a flow rate of 5 μL/min unless otherwise stated. Reagents were injected (35 μL) in the following order: 0.05 M NHS/0.2 M EDC mixture, streptavidin (150−300 μg/mL) in 20 mM acetic acid (pH 4.0), and 0.1 M ethanolamine (pH 8.5). The amount of immobilized streptavidin was typically between 2000 and 4000 RU. The biotinylated derivatives of TGF-α were diluted in HBS [20 mM Hepes (pH 8.0), 150 mM NaCl, 3.4 mM EDTA, and 0.05% Tween 20] and repeatedly injected over the streptavidin surface until a desired amount was immobilized (ranging from 50 to 1000 RU). For binding and kinetics analysis, the dialyzed EGFR-ED was diluted in HBS and injected over the TGF-α surface at different concentrations at a flow rate of 5 μL/min. The TGF-α surface was regenerated by injecting 4 μL of 10 mM HCl.

Analysis of SPR (BIAcore) Measurements. Sensorgrams were analyzed by linearization of the data with BIAevalu-

ation 1.0 (Pharmacia), by nonlinear least-squares curve-fitting with integrated rate equations by use of BIAevaluation 2.1 software (Pharmacia), and by numerical integration using the SP*Revolution* software developed in our laboratory (freely available on the Internet http://www.bri.nrc.ca/csrg/equip.htm#biacore).

Mathematical Modeling and Parameter Estimation with SPRevolution. The various models were transposed into differential equations by making a mass balance on all species present in the dextran matrix. For instance, the simple bimolecular interaction model leads to the following equations:

$$\frac{d\{\text{free}\}}{dt} = -k_a\{\text{free}\}\,[\text{sol}] + k_d\{\text{bound}\} \quad (1)$$

$$\frac{d\{\text{bound}\}}{dt} = k_a\{\text{free}\}\,[\text{sol}] - k_d\{\text{bound}\} \quad (2)$$

with, at $t = 0$,$\{\text{free}\} = \{\text{free}\}_{t=0}$ and $\{\text{bound}\} = 0$. {free} and {bound} refer to the concentrations of free TGF-α and ligand−receptor complex, respectively, per unit volume of solid phase. [sol] refers to the concentration in solution of EGF receptor. It is assumed that the flow in the cell is sufficiently high so that there is no depletion of EGF receptor in solution and its concentration remains constant.

This set of nonlinear differential equations was solved numerically by an adaptive step-size Runge−Kutta method (*15*). The resulting routine was used in a nonlinear regression program with Marquardt's algorithm (*16*) to estimate the values of the constants from experimental data. The same process was applied to all the models that were tested. In the case of the fast binding followed by a slower conformational change (Figure 9C), the following set of equations was used:

$$\frac{d\{\text{free}\}}{dt} = -k_{a1}\{\text{free}\}[\text{sol}] + k_{d1}\{\text{bound1}\} \quad (3)$$

$$\frac{d\{\text{bound1}\}}{dt} = k_{a1}\{\text{free}\}[\text{sol}] - k_{d1}\{\text{bound1}\} + k_{d2}\{\text{bound2}\} - k_{a2}\{\text{bound1}\} \quad (4)$$

$$\frac{d\{\text{bound2}\}}{dt} = k_{a2}\{\text{bound1}\} - k_{d2}\{\text{bound2}\} \quad (5)$$

with, at $t = 0$, $\{\text{free}\} = \{\text{free}\}_{t=0}$ and $\{\text{bound1}\} = \{\text{bound2}\} = 0$, where {bound1} and {bound2} refer to the concentrations of unrearranged and rearranged ligand−receptor adducts, respectively.

For each model, the kinetic parameters and the active quantity of ligand bound to the matrix were considered as global parameters for a given set of curves integrated globally. Moreover, two local parameters were added for each curve to take into account the bulk effect at the beginning of the wash-on and wash-off phases, respectively (see the SP*Revolution* software manual for more details about curve preparation and kinetic models).

Evaluation of the Goodness of Fit for the Various Kinetic Models. For each set of residuals (difference between the experimental values and the values calculated by numerical integration for each kinetic model), three statistical values were calculated:

(1) *Standard Deviation of the residuals.* $SD = [\Sigma(Res_i - Res_{av})^2/(n-1)]^{1/2}$, where Res_i and Res_{av} are the values of the i^{th} residual (difference between the calculated and the experimental point) and the average residual value and n is the number of points.

(2) *+ or − Signs Statistic (Z1) (17).* Each residual is replaced by its sign value (+ or -) and the following statistic is then calculated on the newly created data set:

$$Z_1 = [n\,(R_1 - 1) - 2n_1n_2]/[2n_1n_2(2n_1n_2 - n)/(n-1)]^{1/2}$$

where R_1 is the number of positive runs, n_1 is the + number, and n_2 is the − number. Assuming that the residuals are independent, the above statistic follows a Normal law with a mean equal to 0 and a variance equal to 1.

(3) Run Up and Down Statistic (Z2) (17). By use of the residuals set $x(i)$, a new set of data, y, is created with $y(i) = x(i) - x(i+1)$. As for the above test, each y value is then replaced by its sign value (+ or −). If we call $R2$, the number of positive $y(i)$ of the runs, then the statistic $Z2 = \{R2 - [(2n-1)/3]/[16n - 29)/90]^{1/2}$ also follows a normal distribution whose mean = 0 and variance = 1 if the residuals are independent.

RESULTS

Characterization of the Biotinylated Derivatives of TGF-α. To generate a homogeneous, oriented sensor chip surface, we decided to take the approach of biotinylating TGF-α, separating the biotinylated derivatives, and immobilizing each of them on a streptavidin surface. The reaction between NHS-SS-biotin and TGF-α yields a mixture of biotinylated derivatives that can be separated by reverse-phase HPLC on a C-18 column. The TGF-α molecule contains two free amino groups, one at the N-terminus and one on the lysine at position 29. The presence of two sites for biotinylation on the TGF-α molecule predicts the possibility of generating three different biotinylated derivatives: one monobiotinylated at the N-terminus, one monobiotinylated at lysine 29, and one dibiotinylated at both amino groups. As expected, in addition to unbiotinylated TGF-α, three major peaks were separated by HPLC (data not shown). The molecular masses of unbiotinylated TGF-α and of the three different peaks were analyzed with a Lasermat mass analyzer (Finnigan Mat) and determined to be approximately 5558 (unbiotinylaled TGF-α), 5960 (peak 1), 5944 (peak 2), and 6329 (peak 3) Da. Considering that each addition of a S-S-biotin molecule on the TGF-α molecule will result in an increase in molecular mass of 382 Da, we can conclude that peak 1 and peak 2 are monobiotinylated and that peak 3 is dibiotinylated. To determine which peaks contained derivatives that were biotinylated at the N-terminus, they were subjected to N-terminal Edman degradation. Peaks 2 and 3 were resistant to Edman degradation, indicating the presence of a biotin molecule at the N-terminus. Peak 1 was not protected from Edman degradation, confirming the absence of biotin at the N-terminus. We therefore conclude that peak 1 is biotinylated at lysine 29, peak 2 is biotinylated at the N-terminus, and peak 3 is biotinylated both at the N-terminus and at lysine 29.

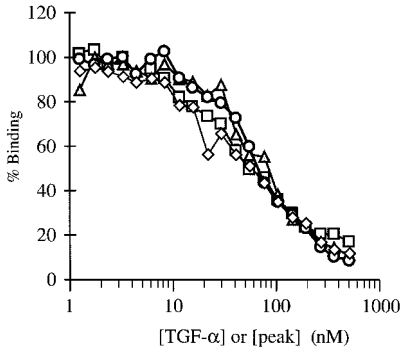

FIGURE 1: Competition of ^{125}I-EGF binding to the EGFR-ED by biotinylated derivatives of TGF-α. In a microtiter plate assay, 3 nM purified EGFR-ED was incubated with 15 nM ^{125}I-EGF in the presence of varying concentrations of unmodified TGF-α (◇), TGF-α biotinylated at the N-terminus (△), TGF-α biotinylated at lysine 29 (□) or TGF-α biotinylated at both the N-terminus and lysine 29 (○). The results are expressed as percent of binding in the absence of competitor.

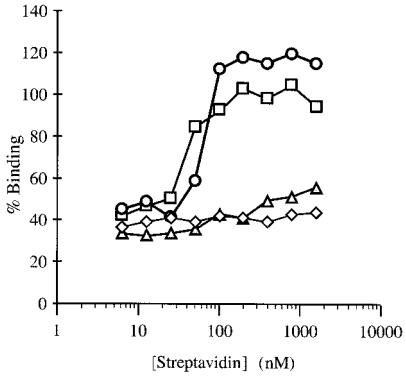

FIGURE 2: Effect of streptavidin on the competition of ^{125}I-EGF binding to the EGFR-ED by biotinylated derivatives of TGF-α. Unmodified TGF-α or the biotinylated derivatives of TGF-α (150 nM) were preincubated with increasing concentrations of streptavidin (ranging from 6 to 1500 nM). The mixtures were then incubated with 3 nM purified EGFR-ED and 15 nM ^{125}I-EGF. Competition curves are presented for unmodified TGF-α (◇), TGF-α biotinylated at the N-terminus (△),TGF-α biotinylated at lysine 29 (□) or TGF-α biotinylated at both the N-terminus and lysine 29 (○).

Analysis of the Interaction of the EGFR-ED with the Three Biotinylated Derivatives of TGF-α in the Absence and Presence of Streptavidin by an ^{125}I-EGF Competition Assay. Our strategy for the immobilization of the TGF-α molecule on the BIAcore CM5 sensor chip surface involves the interaction of biotinylated TGF-α with immobilized streptavidin. To test whether the presence of the biotin on the TGF-α molecule affects its ability to bind in solution to the EGFR-ED, we assayed the ability of TGF-α and the different biotinylated derivatives to compete for the binding of ^{125}I-EGF to the purified EGFR-ED. Figure 1 shows that the three biotinylated derivatives are able to compete for ^{125}I-EGF binding to the EGFR-ED with the same IC_{50} (50 nM) as the unmodified TGF-α, demonstrating that the presence of biotin at the N-terminus or on the lysine at position 29 did not interfere with the binding in solution to the EGFR-ED.

To mimic the surface of the sensor chip where the biotinylated derivatives of TGF-α will be bound to streptavidin, we tested if prebinding of streptavidin to the biotinylated TGF-α derivatives would affect their binding to the EGFR-ED in solution. Figure 2 shows that unbiotinylated TGF-α as well as the N-terminally biotinylated TGF-α derivative was able to compete for ^{125}I-EGF binding to the EGFR-ED even in the presence of excess streptavidin. In contrast, the ability of the two TGF-α derivatives biotinylated at lysine 29 to compete for ^{125}I-EGF binding to the EGFR-ED was inhibited by streptavidin in a dose-dependent manner, with a complete loss of competition at 100 nM streptavidin. Streptavidin alone had no effect on the binding of ^{125}I-EGF to the EGFR-ED (data not shown). These experiments indicate clearly that the derivatives which are biotinylated on lysine 29 are sterically hindered by the presence of a streptavidin molecule at this position and can no longer bind to the EGFR-ED molecule in solution.

Surface Plasmon Resonance Analysis of the Interaction of the EGFR-ED with the Three Biotinylated Derivatives of TGF-α. Figure 3 shows the sensorgrams resulting from the interaction of the EGFR-ED with the three biotinylated derivatives of TGF-α that were captured on streptavidin surfaces. The EGFR-ED interacted only with the derivative that was monobiotinylated at the N-terminus (Figure 3C) and failed to interact with the derivative that was monobiotinylated at lysine 29 (Figure 3A) and the derivative that was dibiotinylated at the N-terminus and lysine 29 (Figure 3B). The inability of the EGFR-ED to interact with the two derivatives of TGF-α that are biotinylated at lysine 29 when captured on the streptavidin sensor chip is consistent with the steric effect of streptavidin that was observed in the ^{125}I-EGF competition assay (Figure 2). The interaction of the EGFR-ED with the N-terminally monobiotinylated TGF-α derivative was blocked by preincubating the EGFR-ED either with an excess of TGF-α or with anti-receptor antibodies that are known to block the binding of TGF-α (data not shown). A control streptavidin surface was used to rule out nonspecific binding of EGFR-ED and also to show that the bulk refractive index change due to the EGFR-ED solution was low (Figure 3D).

Analysis of the Interaction of EGFR-ED with the N-Terminally Biotinylated TGF-α by the Linearization Method and the Integrated Rate Equation Method. We further analyzed the kinetics of the interaction between the EGFR-ED and the TGF-α derivative that was monobiotinylated at the N-terminus. Figure 4A represents a set of typical sensorgrams, after blank subtraction, in which different concentrations of the purified EGFR-ED were flowed over the TGF-α surface. To determine whether the data fit a simple bimolecular or Langmuir interaction (A + B yields AB), the results were analyzed by linearizing the data as previously described (*5*). From the wash-on phase, the apparent k_a can be calculated by first plotting dR/dt against R for each EGFR-ED concentration (Figure 4B). The slope of each line (k_s) is then plotted against the EGFR-ED concentration (Figure 4C) and the slope of this line yields an apparent k_a. Although it is obvious that the plot of dR/dt against R is not linear, even when only 10 s of data was used (94.5−104.5 s, 4 s after the start of the injection), an average apparent k_a can be estimated as $(8.6 \pm 5.2) \times 10^4$ M^{-1} s^{-1}. This is the mean ± the standard deviation of 34 experiments, which included different preparations of EGFR-ED and biotinylated TGF-α and different surface loading. The apparent k_d was calculated from the wash-off phase by using a plot of ln (R_1/R_n) against time (Figure 4D). Although

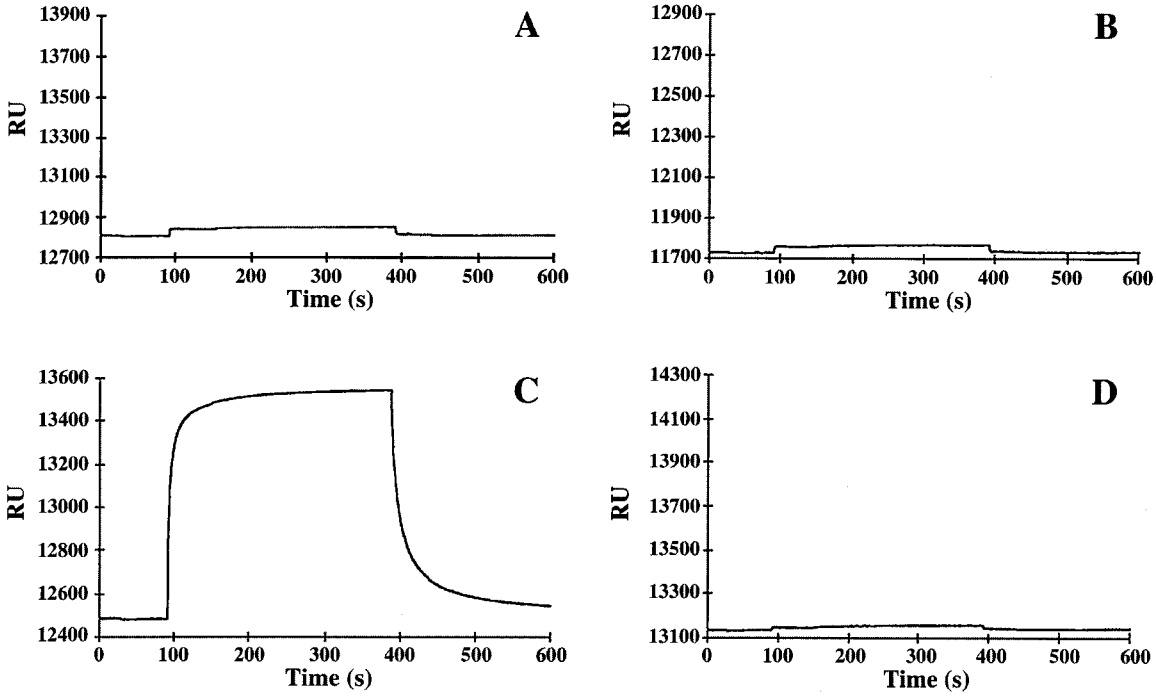

FIGURE 3: SPR analysis of the interactions of EGFR-ED with the three biotinylated derivatives of TGF-α. The biotinylated derivatives of TGF-α were repeatedly injected over independent streptavidin surfaces until 200−300 resonance units (RU) of biotinylated TGF-α was captured. Purified EGFR-ED dialyzed against PBS and diluted in HBS to the desired concentration was injected over the different surfaces: (A) TGF-α biotinylated at lysine 29; (B) TGF-α biotinylated at both lysine 29 and at the N-terminus; (C) TGF-α biotinylated at the N-terminus; (D) streptavidin alone.

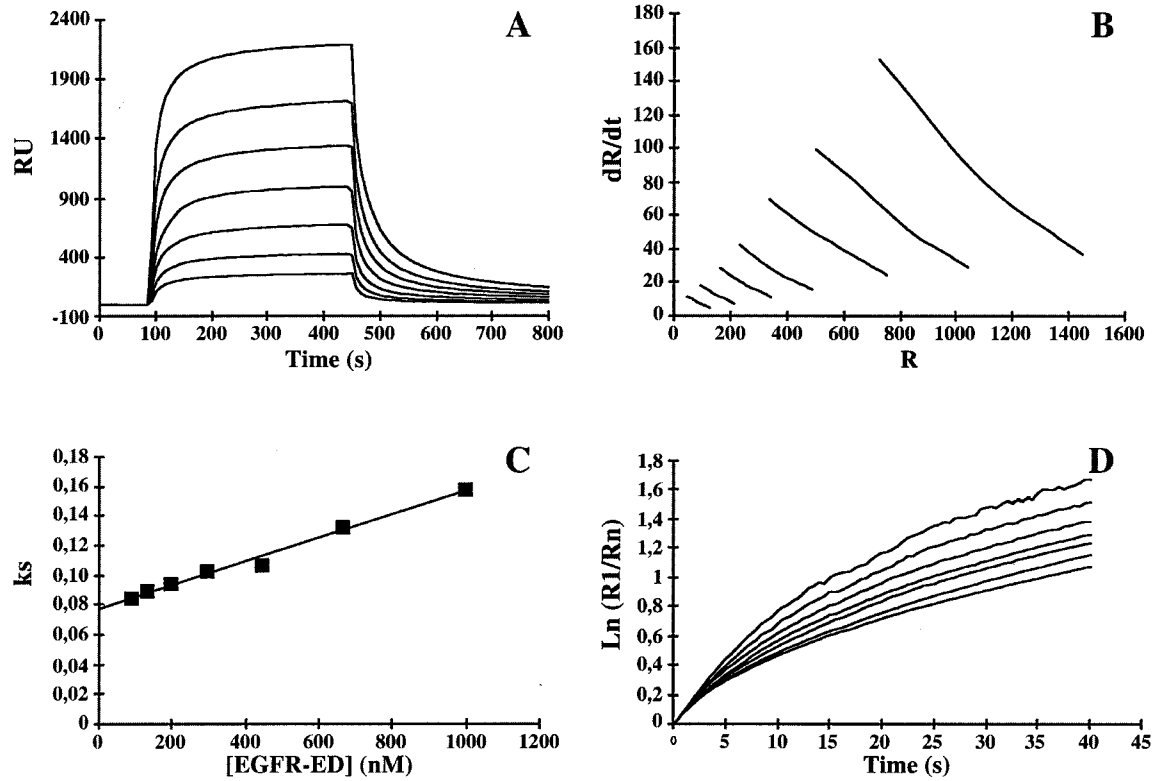

FIGURE 4: Linear analysis of the interaction of the purified EGFR-ED with immobilized TGF-α biotinylated at the N-terminus. Purified EGFR-ED varying in concentration from 88 to 1000 nM was injected over the TGF-α surface. An aliquot (25 μL) of each EGFR-ED concentration was injected at a flow rate of 5 μL/min. (A) Overlay plot of the interaction between 88 and 1000 nM EGFR-ED and 810 RU of TGF-α captured on the surface. Calculation of the k_a was as follows: (B) Linear transformation of the association phase was obtained by plotting dR/dt against the response for a 10 s period beginning at 4 s after the start of the injection. (C) The slope (k_s) of each line was then plotted against EGFR-ED concentration. The slope of this line gives the apparent k_a. Calculation of the k_d was as follows: (D) The data from the dissociation phase are linearized by plotting $\ln(R_1/R_n)$ against time. The slope of this line then gives the apparent k_d.

once again this treatment of the data failed to give a straight line, an apparent k_d was estimated to be 0.06 ± 0.02 s^{-1} when the data from the first 5 s following the end of the injection was used. The data were also analyzed by Scatchard

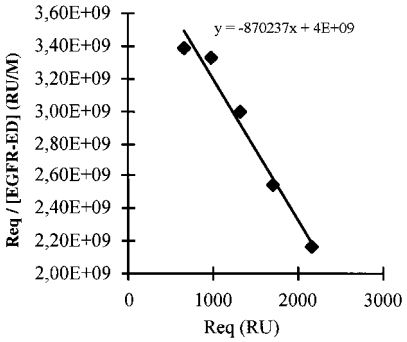

FIGURE 5: Scatchard analysis. R_{eq} (resonance units at the plateau) for each EGFR-ED concentration (as in Figure 4A) was corrected for the bulk refractive index contribution by use of the steptavidin control surface. The slope of the Scatchard plot (R_{eq}/concentration against R_{eq}) gives the apparent K_{Aeq}.

analysis (Figure 5) and an apparent K_{Deq} of 1040 ± 331 nM was estimated. This is similar to the K_{Deq} calculated from the rate constants derived from the linearization of the wash-on and wash-off phases (k_d/k_a), which equals 698 nM.

The data were also analyzed by the integrated rate equation method using the BIAevaluation 2.1 software. This method allows the analysis of both homogeneous and heterogeneous kinetics. Homogeneous binding kinetics describe a homogeneous single-site interaction between two molecules A and B (A + B yields AB). In contrast, heterogeneous binding kinetics describe parallel interaction kinetics in which the observed response is the sum of the responses for binding of analyte (defined as the species in solution) to independent ligand sites (defined as the species coupled to the surface) (A + B_1 + B_2 yields AB_1 + AB_2). The experimental data were analyzed with both homogeneous and heterogeneous binding kinetic models. For the analysis of both the wash-off and the wash-on phases, we found that the experimental data were better represented by the heterogeneous model (Figure 6B,D) than by the homogeneous model (Figure 6A,C). The apparent association and dissociation rate constants that were extrapolated for the heterogeneous model are listed in Table 1. Both apparent association constants (k_{a1} and k_{a2}) increase with decreasing concentration of EGFR-ED, which indicates, however, that this model is not valid.

Deviations from a simple model may be explained either by a more complex biological interaction or by nonoptimized experimental conditions. The latter can result in physical effects such as (1) heterogeneity of the coupled ligand, (2) rebinding of dissociating analyte molecules rather than their removal by the flow, (3) mass transport limitations that occur when the transportation kinetics through the unstirred layer over the surface are slow compared to the binding kinetics, and (4) parking problems, which refers to masking of potential ligand binding sites by previously formed complexes (*8*). Heterogeneity of the coupled ligand can be eliminated by using an oriented ligand surface, while rebinding effects and mass transport limitations can be minimized by increasing the flow rate. Finally, parking problems can be eliminated or at least reduced by decreasing the quantity of ligand coupled to the matrix.

Optimization of Experimental Conditions for Kinetic Analysis. Before evaluating more complex kinetic models, we optimized the experimental design by testing for and

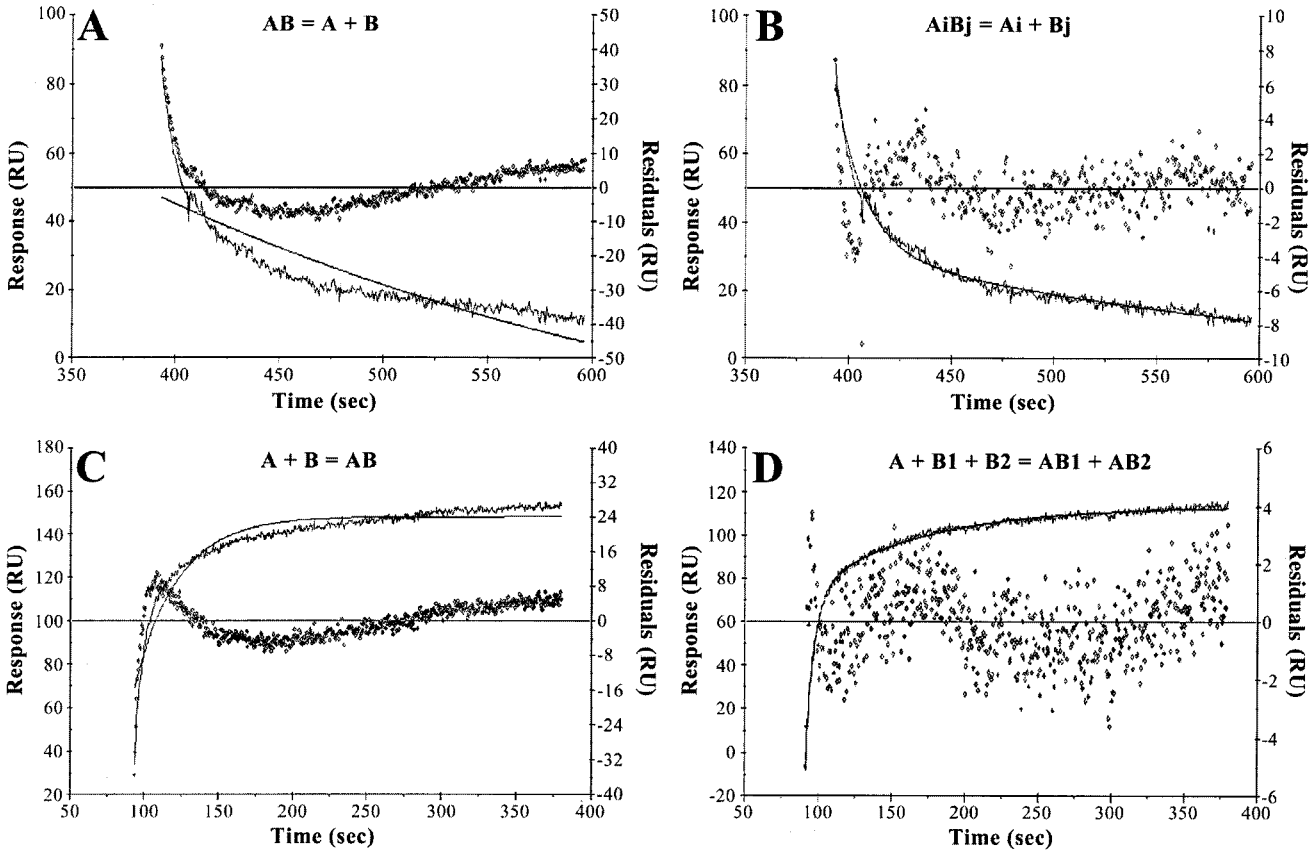

FIGURE 6: Nonlinear least-squares analysis by the integrated rate equation method (BIAevaluation 2.1). EGFR-ED (351 nM) was injected over a surface with 59 RU of immobilized TGF-α. Curve fits and residuals obtained from the analysis of the sensorgram with the following models: (A) homogeneous dissociation, (B) heterogeneous dissociation, (C) homogeneous association and (D) heterogeneous association.

Table 1: Kinetic and Equilibrium Constants Obtained from the Analysis of the TGF-α/EGFR-ED Interaction for a Heterogeneous Model by BIAevaluation 2.1 (Integrated Rate Equation Method)

[EGFR-ED] (nM)	k_{a1} (M^{-1} s^{-1}) $\times 10^{-3}$	k_{d1} (s^{-1}) $\times 10^{2}$	k_{a2} (M^{-1} s^{-1}) $\times 10^{-3}$	k_{d2} (s^{-1}) $\times 10^{3}$	K_{D1} (μM)	K_{D2} (μM)
1185	100 ± 1.6	6.5 ± 0.1	8.67 ± 0.28	3.59 ± 0.12	0.650	0.415
527	185 ± 4.3	7.0 ± 0.2	14.8 ± 0.51	4.12 ± 0.15	0.378	0.277
351	287 ± 9.6	6.7 ± 0.2	27.2 ± 0.80	3.57 ± 0.15	0.233	0.132

eliminating or minimizing the unwanted phenomena listed above. Heterogeneity of the ligand may arise during the immobilization step if more than one coupling site is present on the ligand molecule. To avoid this, only the HPLC-purified N-terminally monobiotinylated TGF-α derivative was used for kinetic studies. The use of a low-loaded surface (less than 60 RU of bound material) and an increase in the flow rate from 5 to 50 μL/min did not improve the data analysis (data not shown), as would have been the case if mass transport limitations were present during either the wash-on or the wash-off phases. In addition, injection of EGF in solution during the wash-off phase did not change the dissociation rate of the interaction (data not shown), which excludes a rebinding effect since the presence of excess EGF during the dissociation phase would have competed rebinding of EGFR-ED and would have affected the dissociation part of the sensorgram. Finally, the issue of a parking problem was addressed. Parking may be observed especially when a high molecular weight analyte interacts with a low molecular weight immobilized ligand and also becomes more prevalant when the quantity of ligand immobilized to the surface is high because of steric problems arising from the closer proximity of the molecules. A study was carried out with 11 different surfaces in which varying concentrations of N-terminally biotinylated TGF-α were immobilized to surfaces with different amounts of streptavidin in order to vary the ratio of streptavidin to TGF-α. Surface activity was measured by Scatchard analysis. Figure 7 summarizes the percentage of surface TGF-α that is active, plotted against the total amount of streptavidin and TGF-α that were coupled. Given that the streptavidin molecule has four binding sites for biotin, when the TGF-α to streptavidin ratio is greater than 1:1, the possibility of having more than one molecule of TGF-α bound to the same streptavidin molecule increases. Taking into account the size of the EGFR-ED molecule, such a situation may provoke steric hindrance and consequently parking problems as emphasized by O'Shannessy and Winzor (*8*). Indeed, a decrease of surface activity was observed when the molar ratio of biotinylated TGF-α to streptavidin increased. To minimize this effect, we used surfaces where the ratio of ligand/streptavidin was the lowest possible (e.g., much lower than 1:1) while still being able to detect a response as shown in Figure 8.

Global Analysis by SPRevolution. Data analysis by the linearization and integrated rate equation methods clearly showed that the data generated for the interaction between immobilized TGF-α and EGFR-ED do not follow a simple bimolecular interaction model even when experimental conditions have been optimized. To test more complex models, the data were further analyzed by a software program developed in our laboratory, SP*Revolution*, that uses numerical integration techniques to perform global analysis of BIAcore-generated sensorgram sets.

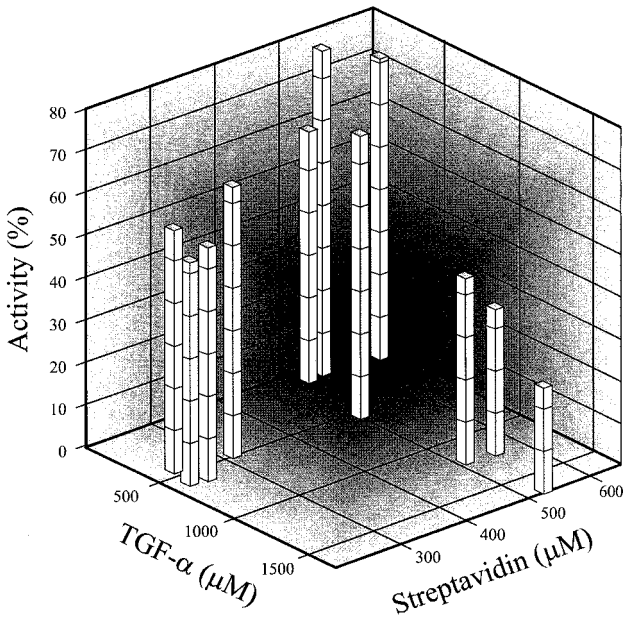

FIGURE 7: Effect of immobilized streptavidin and biotinylated TGF-α concentrations on the percent of active TGF-α on the surface. For each surface, the amount of streptavidin on the surface was determined from the baseline change that occurred during the coupling step. Similarly, the amount of total immobilized TGF-α was determined from the RU baseline change that occurred when the N-terminally biotinylated TGF-α was injected over the streptavidin surface. The amount of active TGF-α on the surface was then determined by injecting concentrations of EGFR-ED ranging from 234 to 1185 nM and by subsequent Scatchard analysis. The results are expressed as the percent of TGF-α on the surface that is active versus the concentrations of immobilized streptavidin and TGF-α.

With the numerical integration SP*Revolution* software program, the data were prepared as follows: Blank sensorgrams, generated by injecting EGFR-ED solution over a mock surface where streptavidin but not TGF-α was immobilized, were subtracted from the corresponding data sensorgrams by exactly aligning the beginning of the wash-on and wash-off phases. The curves resulting from these subtractions were then reduced to 500 points evenly selected from the wash-on and wash-off phases. For each different surface, the curves were then globally fitted by the different models illustrated in Figure 9. Model A represents a situation where mass transport limitation in solution is coupled to a simple Langmuirian interaction. Model B assumes that two different populations of biotinylated TGF-α are present in the matrix. Model C includes a conformational change or transformation of the receptor−ligand complex after binding, which has been observed in solution (*9*). Models D and E both depict dimerization models: the first one assumes the ability of one receptor molecule to bind to a preformed ligand−receptor complex (1:2 stoichiometry), whereas the second is characterized by the ability of the receptor−ligand complex to form dimers (2:2 stoichiometry). Indeed, it has been shown

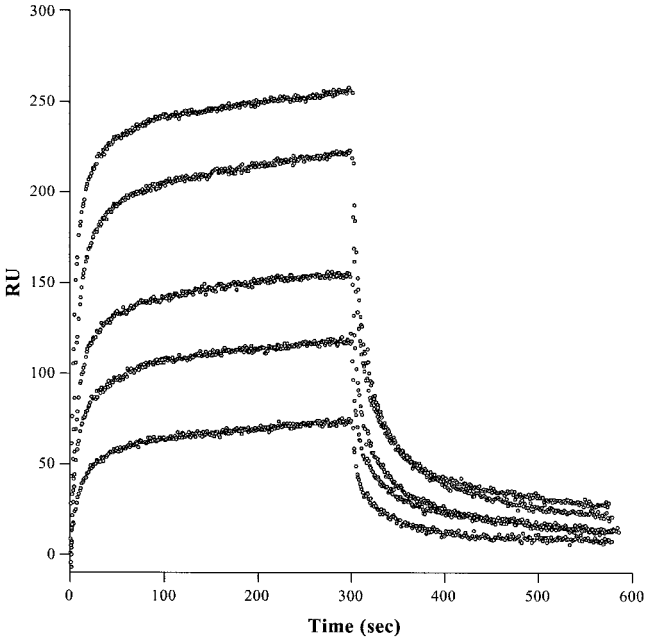

FIGURE 8: Optimized data set for the interaction between EGFR-ED and TGF-α. Different concentrations of EGFR-ED ranging from 234 nM to 1185 nM were injected over a surface with 59 RU of immobilized biotinylated TGF-α. An aliquot (25 μL) of each EGFR-ED solution was injected at a flow rate of 5 μL/min. After blank subtraction, each curve was reduced to 500 points, evenly selected, as described in the text.

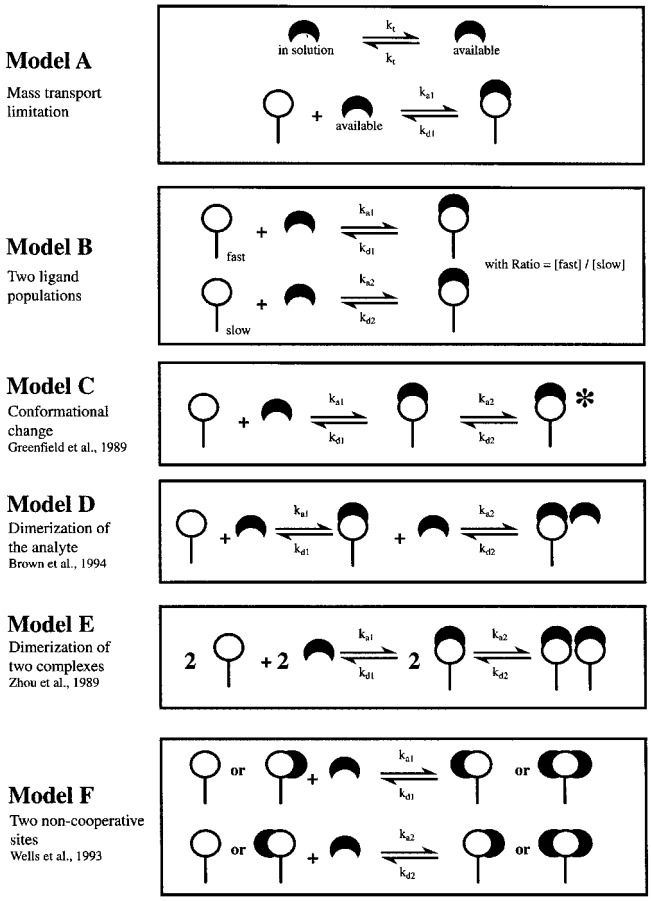

FIGURE 9: Schematic representation of kinetic models. Model A represents a mass transport limitation situation, and model B depicts heterogeneity of the coupled ligand. All the other models (C−F) represent more complex biological interaction mechanisms and have been chosen according to the references given beside the schematic representation. For details, see text.

for EGFR-ED that dimerization can occur in solution (*10*, *11*) and that it can occur in the dextran matrix of the BIAcore (*18*). Model F depicts the case where the ligand has two sites interacting with the receptor as occurs for the growth hormone receptor (*12*). For every model tested, the program was allowed not only to vary the kinetic parameters but also to vary the active quantity of TGF-α, which can be correlated to the *k* (activity) parameter introduced by Karlsson and Fält (*19*). Additionally, for each sensorgram in the data set, two more local parameters were added to eliminate, or at least reduce, the offset artifacts introduced because of the subtraction step in the wash-on and wash-off phases. The data that we analyzed were generated with five concentrations of EGFR-ED (ranging from 234 to 1185 nM) over a surface where 59 RU of biotinylated TGF-α was coupled (Figure 8). Integration results are shown as residuals (difference between the experimental and calculated data points) in Figure 10 and the related kinetic constants are listed in Table 2. One can evaluate the relative goodness of the fit for different kinetic models applied to the same data set by taking into consideration the trends in the residuals. If a kinetic model adequately depicts the biomolecular interactions, one expects that the difference between the calculated and the experimental points will be minimal and that the residuals will be normally distributed around a zero value. That is, a significantly large amplitude of the residuals, long series of positive or negative points, or long series of ascending or descending points will be absent from the residual plot. Thus, the standard deviation value and the Z_1 and Z_2 statistics are appropriate to quantitatively discriminate between the different proposed models: the lower these three values, the better the goodness of the fit.

The use of numerical integration data analysis to fit a model that includes a mass transport limitation coupled to a simple bimolecular interaction lead to a poor quality fit (Figure 10 and Table 2). This supports our previous conclusion that mass transport artifacts were absent from this series of experiments.The residuals (Figure 10) and their associated standard deviation, Z_1, and Z_2 values (Table 2) indicate that models C and B appear to best fit the experimental curves. However, model B (two ligand populations in the matrix) is not valid because of the overparametrization that was evident in its associated correlation matrix coefficients (data not shown). This conclusion is corroborated by the previous data analysis done with the integrated rate equation method (BIAevaluation 2.1). Additionally, it would have been suprising if this model was valid since care was taken to generate an oriented-ligand surface by a streptavidin/biotin approach.

The conformational change model that was found to best depict the TGF-α/EGFR-ED interaction is the simplest type of conformational change model (Figure 9) that can be proposed. Two more complex conformational change models were tested. The first one includes the addition of a step corresponding to the direct and irreversible dissociation of the rearranged complex to unbound ligand and analyte [RL (rearranged) ⟹ R + L]. The second model is the same as the first, except that the added step is reversible [RL (rearranged) ⟺ R + L]. In both cases, the goodness of the fit was not increased beyond that of the simpler conforma-

Table 2: Global Analysis of the Biotinylated TGF-α/EGFR-ED Interaction Testing Different Kinetic Models with SP*Revolution* Software (Numerical Integration Method)[a]

	models tested					
	A	B	C	D	E	F
k_{a1} (M^{-1} s^{-1})	6.1×10^4	8.1×10^4	6.0×10^4	7.5×10^4	8.4×10^4	1.2×10^5
95% confidence	2.6×10^3	3.5×10^3	2.0×10^3	3.5×10^3	3.2×10^3	6.7×10^3
k_{d1} (s^{-1})	5.9×10^{-2}	1.1×10^{-1}	1.2×10^{-1}	6.7×10^{-2}	8.1×10^{-2}	1.3×10^{-1}
95% confidence	2.6×10^{-2}	2.8×10^{-3}	3.6×10^{-3}	1.8×10^{-3}	2.1×10^{-3}	4.6×10^{-3}
k_{a2} (M^{-1} s^{-1})	n/a	9.6×10^3	4.2×10^{-3}[b]	8.8×10^{-1}	5.9×10^{-2}	4.0×10^3
95% confidence	n/a	4.9×10^2	2.3×10^{-4}	4.6×10^{-2}	3.1×10^{-3}	3.2×10^2
k_{d2} (s^{-1})	n/a	7.7×10^{-3}	1.2×10^{-2}	3.7×10^{-3}	5.2×10^{-3}	1.5×10^{-2}
95% confidence	n/a	4.1×10^{-4}	5.4×10^{-4}	3.3×10^{-4}	3.7×10^{-4}	5.5×10^{-4}
k_t (s^{-1})	1.3	n/a	n/a	n/a	n/a	n/a
95% confidence	0.5	n/a	n/a	n/a	n/a	n/a
ratio [fast]/[slow]	n/a	3.8	n/a	n/a	n/a	n/a
95% confidence	n/a	0.2	n/a	n/a	n/a	n/a
surface activity (RU)	18.5	36.3	44.7	24.1	25.6	24.7
95% confidence	1.01	1.0	1.1	0.7	0.56	0.8
standard deviation (RU)	8.7	3.1	3.1	4.9	4.1	3.8
+ and − test (Z_1)	41.0	24.8	20.5	37.5	32.9	30.0
Run up and down test (Z_2)	3.7	1.9	1.1	2.6	2.1	2.1

[a] Data were generated by injecting several concentrations of EGFR-ED (234−1185 nM) over a surface where 59 RU of biotinylated TGF-α was coupled. [b] The unit for this association rate constant is s^{-1}.

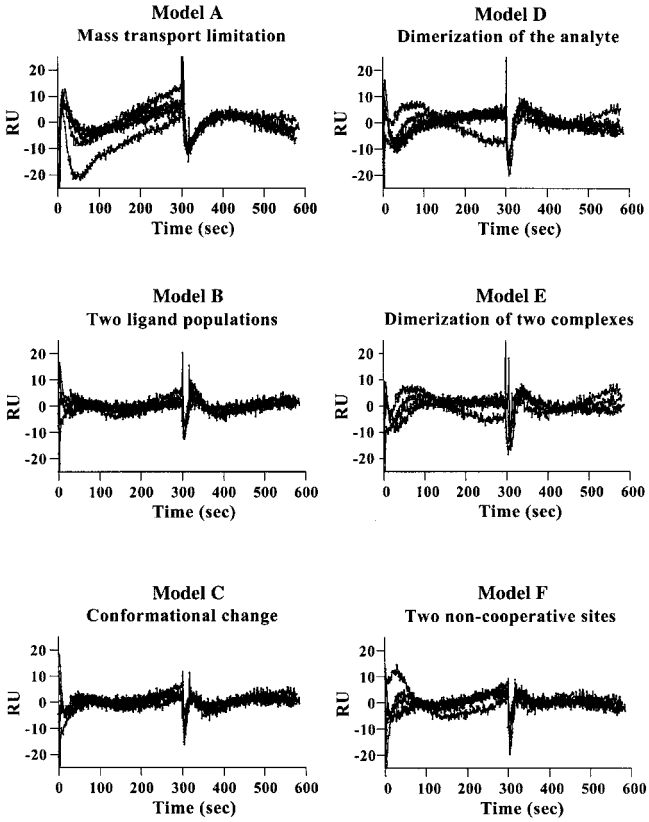

FIGURE 10: Residuals obtained by global analysis of the EGFR-ED/biotinylated TGF-α interaction data. Residuals are the difference between the experimental and the calculated data points. The results indicate that models B and C best fit the data. For further explanation, see text.

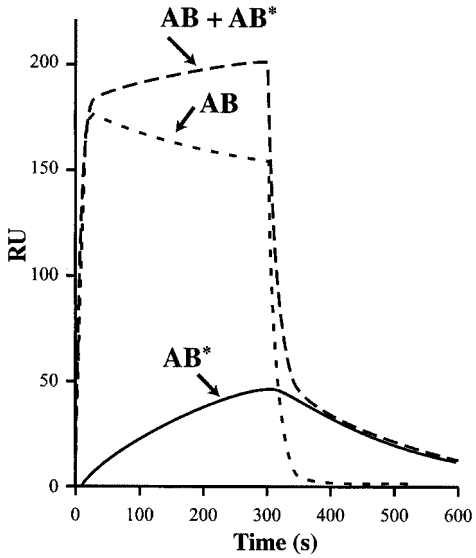

FIGURE 11: Simulation of the time-dependent variation of the receptor/ligand complexes. The simulation was done with the same Runge−Kutta algorithm as in SP*Revolution* and the parameters related to the conformational change model as listed in Table 2. The concentration of injected EGFR-ED was set as 600 nM and the TGF-α quantity as 59 RU. The sum of the populations of unrearranged receptor (denoted AB) and of rearranged one (AB*) corresponds to the signal that would have been recorded (denoted AB + AB*) by performing such an injection and assuming a conformational change kinetic interaction.

tional change model, and both models were overparametrized as judged by the correlation matrixes. This indicates that the addition of these steps does not result in a better depiction of the TGF-α/EGFR-ED interaction (data not shown).

Using the kinetic parameters that were determined by global analysis for the conformational change model (see Table 2), one can calculate an apparent thermodynamic K_{deq}, defined as $[k_{a1}/k_{d1}(1 + k_{a2}/k_{d2})]^{-1}$, to be equal to 1489 nM. Using these parameters and the quantity of active TGF-α coupled to the surface, one can also simulate the quantities of the rearranged and unrearranged receptor/ligand complexes over time. By looking at Figure 11, which simulates the time dependence of complex formation when a 600 nM receptor solution is injected over a 59 RU TGF-α surface, it can be seen that the unrearranged receptor/ligand complex is predominant at the early stage of the wash-on phase. Similarly, the unrearranged complex contributes predominantly to the signal in the early part of the wash-off phase. Hence the apparent K_{deq} constant estimated by Scatchard analysis using the plateau values, approximately 1000 nM

(Figure 5), or by using the early parts of the wash-on and wash-off phases with the linearization method, approximately 700 nM (Figure 4), are close to the value determined by the numerical integration technique, even though they did not take into account the kinetic mechanism that best depicts the biological interaction.

DISCUSSION

To study the interaction between TGF-α and EGFR-ED with the BIAcore, the ligand molecule (TGF-α) was immobilized on the sensor chip and EGFR-ED, as the analyte, was injected over the sensor chip surface. Our immobilization strategy was chosen in order to have a ligand surface as homogeneous as possible. TGF-α was biotinylated and the three different biotinylated derivatives were separated by reverse-phase HPLC before being captured separately on different streptavidin surfaces. Solution binding assays and preliminary experiments with the BIAcore proved that, among all the streptavidin-bound biotinylated derivatives of TGF-α, only the derivative monobiotinylated at the N-terminus was able to interact with EGFR-ED (Figures 1−3). NMR studies of the structure of TGF-α in the presence or absence of EGFR-ED support the concept that the N-terminus is not directly involved in receptor binding. Specifically, Hoyt et al. (*20*) demonstrated by analyzing ^{1}H NMR relaxation rates of methyl resonances that the N-terminus of TGF-α remains flexible when bound to EGFR-ED. Additionally, the ^{1}H NMR transferred NOE experiments conducted by McInnes et al. (*21*) confirmed that the N-terminus of TGF-α retains flexibility when bound to EGFR-ED. This hypothesis was reinforced by the latest work of McInness et al. (*22*), which demonstrated, through deletional analysis, that the N-terminus does not contribute directly to binding, although it is significant in terms of stabilizing the native fold of TGF-α.

In addition to eliminating direct involvement of the N-terminus of TGF-α in receptor binding, these NMR studies showed the importance of residues in the A and C loop of TGF-α as being part of the major binding interface with the receptor. It is then not unexpected that the presence of streptavidin bound to lysine 29 masks many of the residues of TGF-α that are involved in binding.

Our preliminary kinetic analysis revealed that, as observed for many systems studied with BIAcore technology, the EGFR-ED/TGF-α interaction failed to be represented as a simple bimolecular interaction. This was clearly demonstrated in our attempt to analyze the experimental data by linearization methods (Figure 4) or curve-fitting with a single rate equation by the BIAevaluation 2.1 software package (Figure 6A,C). Nevertheless, we estimated apparent rate constants for the initial fast association and dissociation steps by linearization. The thermodynamic constant that was calculated from the estimated rate constants (K_{deq} = 698 nM) was in keeping with the equilibrium constant determined by Scatchard analysis using the plateau values (K_{deq} = 1040 nM). Additionally, the apparent thermodynamic K_{deq} that was calculated by global analysis for the conformational change model is equal to 1489 nM. These three K_{deq} values are comparable to the one determined for the EGF and EGFR-ED interaction when EGF was directly immobilized by an amine coupling method (*23*) and are in good agreement with the microcalorimetric estimations and SAXS experiments done by Lemmon et al. (*11*). In contrast, the apparent K_d determined by the ^{125}I-EGF competition assay was approximately 50 nM (Figure 1). This difference likely results from the use of the antibody to immobilize EGFR-ED in the microtiter plates. It is known that bivalent antibodies can capture EGFR as a dimer, and it has also been shown that this type of ligand-binding assay only detects binding to higher affinity dimeric EGFR and not monomeric EGFR (*24*). A better mimic of the plate assay in the BIAcore would be the noncovalent capture of EGFR-ED on a covalently immobilized monoclonal antibody followed by TGF-α injections. Such an experiment has the disadvantage that TGF-α has a much lower molecular weight than EGFR-ED, thus rendering its detection as the analyte difficult.

Deviations from pseudo-first-order kinetics may be explained by phenomena inherent to the design of the BIAcore technology or the experiment itself. These artifacts include heterogeneity of the immobilized ligand, mass transport limitation, rebinding effects, and parking problems (*25*). On the other hand, it is also possible that a more complex kinetic model is required to explain the biological interaction between TGF-α and EGFR-ED.

After optimizing the experimental design and still observing a deviation from the simple model, we tested more complex biological models using numerical integration to globally fit data obtained under optimized conditions. The rationale for choosing the interaction models was based on literature hypotheses. Among all the models tested, the one describing a conformational change in the receptor−ligand complex after binding gave us the best fit (Figure 10, Table 2). The choice of this model was based on the circular dichroism analysis of Greenfield et al. (*9*), which indicates that a conformational change occurs upon EGFR-ED/TGF-α binding. Neither these circular dichroism studies nor our SPR experiments are able to distinguish which one of the interacting species undergoes a conformational change. However, ^{1}H NMR transferred NOE experiments (*21*) and HSQC NMR experiments (McInnes et al., submitted for publication) showed that no major structural rearrangement of TGF-α occurs upon complexation with EGFR-ED. This indicates that the conformational change is more likely to be within the receptor extracellular domain.

On the basis of microcalorimetry titration and SAXS experiments, Lemmon et al. (*11*) proposed that the kinetic mechanism of binding for EGF and EGFR-ED involves the dimerization of two preformed EGF/EGFR-ED complexes. They were unable to distinguish whether this dimerization results from a conformation-driven exposure of a dimerization site on the receptor or is achieved due to ligand bivalency (a bridging ligand molecule). Our results support the conformational change model. The reason we did not detect dimerization of the EGFR-ED/TGF-α complex after the conformational change step could be because the rate constants for this step are rapid and not limiting and therefore are undetectable by the SPR biosensor technology.

Studies by Sherrill and Kyte (*26*, *27*) also question the validity of the bivalent bridging ligand model since an excess of EGF ligand does not inhibit the activation of the EGF receptor even at high concentrations. Moreover, Tanner (*28*) showed that after the removal of EGF from a dimeric complex of full-length EGF receptor, the dimer, which is

still enzymatically active, dissociates over a period of hours, thus excluding the requirement of a bivalent ligand for receptor dimer stabilization.

The concept that a change in conformation of a receptor/ligand complex is required for receptor dimerization and subsequent activation is just emerging as a prevalent theme. Indeed, very recently, it was shown for the erythropoietin receptor/ligand system through crystallographic evidence and an in vivo protein interaction assay (*29*, *30*) that the activation of the complex requires a change in its conformation after ligand binding. Our results, combined with those of others, strongly suggest that, like the erythropoietin receptor, ligand binding to the EGF receptor is followed by a change in the conformation of the receptor, which then promotes its activation.

ACKNOWLEDGMENT

We thank Dr. Anne E. G. Lenferink and Dr. Darrell D. Mousseau for their critical review and comments during the preparation of the manuscript, and France Dumas for technical support.

REFERENCES

1. Carpenter, G., and Cohen, S. (1979) *Annu. Rev. Biochem. 48*, 193−216.
2. Schlessinger, J., and Ullrich, A. (1992) *Neuron 9*, 383−391.
3. Ullrich, A., Coussens, L., Hayflick, J. S., Dull, T. J., Gray, A., Tam, A. W., Lee, J., Yarden, Y., Libermann, T. A., Schlessinger, J., et al. (1984) *Nature 309*, 418−425.
4. Morton, T. A., Myszka, D. G., and Chaiken, I. M. (1995) *Anal. Biochem. 227*, 176−185.
5. Karlsson, R., Michaelsson, A., and Mattsson, L. (1991) *J. Immunol. Methods 145*, 229−240.
6. O'Shannessy, D. J., Brigham-Burke, M., Soneson, K. K., Hensley, P., and Brooks, I. (1993) *Anal. Biochem. 212*, 457−468.
7. Fisher, R. J., and Fivash, M. (1994) *Curr. Opin. Biotechnol. 5*, 389−395.
8. O'Shannessy, D. J., and Winzor, D. J. (1996) *Anal. Biochem. 236*, 275−283.
9. Greenfield, C., Hiles, I., Waterfield, M. D., Federwisch, M., Wollmer, A., Blundell, T. L., and McDonald, N. (1989) *EMBO J. 8*, 4115−4123.
10. Brown, P. M., Debanne, M. T., Grothe, S., Bergsma, D., Caron, M., Kay, C., and O'Connor-McCourt, M. D. (1994) *Eur. J. Biochem. 225*, 223−233.
11. Lemmon, M. A., Bu, Z. M., Ladbury, J. E., Zhou, M., Pinchasi, D., Lax, I., Engelman, D. M., and Schlessinger, J. (1997) *EMBO J. 16*, 281−294.
12. Wells, J. A., Cunningham, B. C., Fuh, G., Lowman, H. B., Bass, S. H., Mulkerrin, M. G., Ultsch, M., and deVos, A. M. (1993) *Recent Prog. Horm. Res. 48*, 253−275.
13. Debanne, M. T., Pacheco-Oliver, M. C., and O'Connor-McCourt, M. D. (1995) *Methods Mol. Biol. 39*, 349−361.
14. Carpenter, G., and Cohen, S. (1976) *J. Cell Biol. 71*, 159−171.
15. Press, W. H., Flannery, B. P., Teukolsky, S. A., and Vetterling, W. T. (1986) *Numerical recipes, the art of scientific computing* Cambridge University Press, Cambridge, England.
16. Marquardt, D. W. (1963) *J. Soc. Indust. Appl. Math. 11*, 431−441.
17. Bradley, J. V. (1968) *Distribution−Free statistical tests*, Prentice-Hall, Inc., Englewood Cliffs, NJ.
18. Myszka, D. G., Arulanantham, P. R., Sana, T., Wu, Z., Morton, T. A., and Ciardelli, T. L. (1996) *Protein Sci.* 5, 2468−2478.
19. Karlsson, R., and Falt, A. (1997) *J. Immunol. Methods 200*, 121−133.
20. Hoyt, D. W., Harkins, R. N., Debanne, M. T., O'Connor-McCourt, M. D., and Sykes, B. D. (1994) *Biochemistry 33*, 15283−15292.
21. McInnes, C., Hoyt, D. W., Harkins, R. N., Pagila, R. N., Debanne, M. T., O'Connor-McCourt, M. D., and Sykes, B. D. (1996) *J. Biol. Chem. 271*, 32204−32211.
22. McInnes, C., Wang, J., Al Moustafa, A. E., Yansouni, C., O'Connor-McCourt, M. D., and Sykes, B. D. (1998) *J. Biol. Chem. 273*, 27357−27363.
23. Zhou, M., Felder, S., Rubinstein, M., Hurwitz, D. R., Ullrich, A., Lax, I., and Schlessinger, J. (1993) *Biochemistry 32*, 8193−8198.
24. Neelam, B., Richter, A., Chamberlin, S. G., Puddicombe, S. M., Murray, M. B., Nandagopal, K., Niyogi, S. K., and Davies, D. E. (1998) *Biochemistry* 37, 4884−4891.
25. O'Shannessy, D. J., Brigham-Burke, M., Soneson, K. K., Hensley, P., and Brooks, I. (1994) *Methods Enzymol. 240*, 323−349.
26. Sherrill, J. M., and Kyte, J. (1996) *Biochemistry 35*, 5705−5718.
27. Sherrill, J. M., and Kyte, J. (1999) *Biochemistry 38*, 3106−3111.
28. Tanner, K. G. (1997) *Biochemistry 36*, 14889−14896.
29. Livnah, O., Stura, E. A., Middleton, S. A., Johnson, D. L., Jolliffe, L. K., and Wilson, I. A. (1999) *Science 283*, 987−990.
30. Remy, I., Wilson, I. A., and Michnick, S. W. (1999) *Science 283*, 990−993.

BI992987R